# COMPARISON OF SIDELOBES OF LIMITED DIFFRACTION BEAMS AND LOCALIZED WAVES

Jian-yu Lu and James F. Greenleaf

Biodynamics Research Unit, Department of Physiology and Biophysics
Mayo Clinic/Foundation
Rochester, MN 55905

## INTRODUCTION

### Limited Diffraction Beams

Limited diffraction beams are a class of non-spreading solutions to the isotropic/homogeneous scalar wave equation. The first limited diffraction beam, called Bessel beam, was discovered by Durnin in 1987.[1] Later, Lu and Greenleaf discovered families of limited diffraction beams[2,3] that include all the limited diffraction beams known previously, in addition to an infinity of new beams. One family of limited diffraction beams has an X-like shape along the beam axis and was termed X wave. X waves are different from the Bessel beam because they have multiple frequencies.[2]

With an infinite aperture and energy, limited diffraction beams would propagate to infinite distance without spreading. Even if produced with a finite aperture and energy, they have a very large depth of field. Because of this advantage, limited diffraction beams could have applications in medical imaging,[4,5] tissue characterization,[6] nondestructive evaluation of materials[7] and other wave related areas such as electromagnetics[8] and optics.[9] A recent review of limited diffraction beams is given in Ref. 10.

### Localized Waves

Although limited diffraction beams have a large depth of field, their sidelobes are larger than conventional focused beams at their focuses. Sidelobes may lower the contrast in medical imaging and increase the sampling volume in tissue characterization.

*Acoustical Imaging, Vol. 21*, Edited by
J.P. Jones, Plenum Press, New York, 1995

Localized waves were first discovered by Brittingham in 1983.[11] They were further developed by Ziolkowski et al.[12,13] and Donnelly et al.[14,15,16] Localized waves are also non-spreading and can propagate with only local deformations in their waveforms. Under ideal conditions, localized waves have lower sidelobes than limited diffraction beams. In this paper, we will study the conditions under which localized waves, specifically, subsonic (or subluminal) localized waves developed by Donnelly et al.,[15] have lower sidelobes.

## X WAVE AND SUBSONIC (SUBLUMINAL) LOCALIZED WAVE

Many limited diffraction beams and localized waves have been discovered.[10] Sidelobes of different limited diffraction beams are similar, they decay in the order of $1/\sqrt{r}$, where $r = \sqrt{x^2 + y^2}$ is a radial distance perpendicular to the beam axis. Sidelobes of localized waves decay in the order of $1/r$. Because sidelobes of localized waves are also similar to each other, for simplicity, we study only the subsonic (or subluminal) localized wave[15] in the following. To study the difference between localized waves and limited diffraction beams, we will use a limited diffraction beam (the zeroth-order X wave[2]) for comparison.

The zeroth-order X wave is given by[2]

$$\Phi_{XBB_0} = \frac{a_0}{\sqrt{(r\sin\zeta)^2 + [a_0 - i(z\cos\zeta - ct)]^2}}, \tag{1}$$

where $\Phi_{XBB_0}$ represents acoustic pressure or velocity potential (or scalar electric or magnetic field strength in electromagnetics), $a_0$ is a constant that determines the decay speed of the high frequency components of the X wave, $\zeta$ is an Axicon angle, $i = \sqrt{-1}$, $z$ is the propagation axis, $t$ is time, and $c$ is the speed of sound. It is seen from Eq. (1) that if $z\cos\zeta - ct =$ constant, $\Phi_{XBB_0}$ will be independent of $z$ and $t$, i.e., the X wave is propagation-invariant.

The subsonic wave obtained by Donnelly[15] has the form of a sinc function

$$\Phi_{Sub}(\vec{r}, t) = \frac{\sin\left[\frac{\xi}{\sin^2\zeta}\sqrt{(z - (c\cos\zeta)t)^2 + (r\sin\zeta)^2}\right]}{\frac{\xi}{\sin^2\zeta}\sqrt{(z - (c\cos\zeta)t)^2 + (r\sin\zeta)^2}} e^{i\frac{\xi\cos\zeta}{\sin^2\zeta}\left(z - \frac{c}{\cos\zeta}t\right)}, \tag{2}$$

where the subscript "Sub" means subsonic (or subluminal), $\xi$ and $\zeta$ are constants. The spectrum of $\Phi_{Sub}(\vec{r}, t)$ can be obtained from Eq. (2)[10]

$$\widetilde{\Phi}_{Sub}(\vec{r}, \omega) = \frac{\pi\sin^2\zeta}{\xi c\cos\zeta} e^{i\left(\frac{\omega}{c} - \xi\right)\frac{1}{\cos\zeta}z} J_0\left(r\tan\zeta\sqrt{\left(\frac{\xi\cos\zeta}{\sin^2\zeta}\right)^2 - \left|\frac{\omega}{c} - \frac{\xi}{\sin^2\zeta}\right|^2}\right), \tag{3}$$

where $0 < \left|\frac{\omega}{c} - \frac{\xi}{\sin^2\zeta}\right| < \frac{\xi\cos\zeta}{\sin^2\zeta}$.

The propagation speed of the peak of the subsonic (or subluminal) wave in Eq. (2) is slower than the speed of sound (or light). This is opposite to the X wave whose peak propagates at a speed that is faster than the speed of sound (or light) (supersonic (or superluminal), see Eq. (1)).[2] It is seen that the frequency spectrum of the subsonic wave in Eq. (3) has limited bandwidth. The peak of the real or imaginary parts of the subsonic wave fluctuates as the wave propagates, which is a common feature of all localized waves (Eq. (2)).[10] This is because the localized waves always contain two propagation terms:

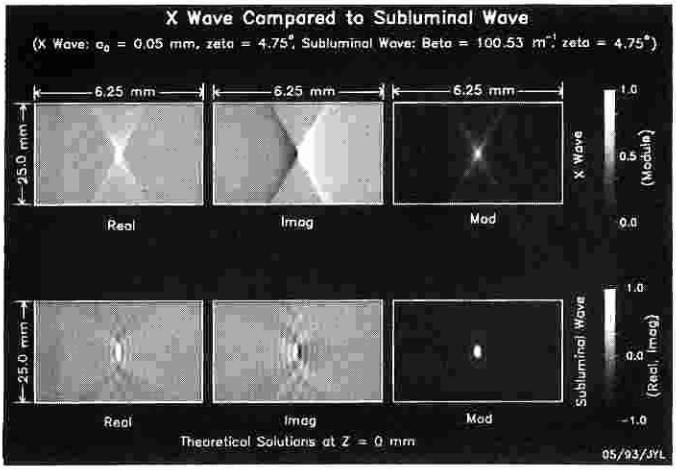


**Figure 1.** Theoretical X waves (top row) and subsonic (or subluminal) waves (bottom row) given by Eqs. (1) and (2) at the axial distance, $z = 0$. The horizontal direction represents time, the distance (6.25 mm) is calculated by assuming the speed of sound is 1500 m/s. The vertical direction is the radial direction and the images shown in the figure are a cross section through the wave axis. The dimension of each image is 6.25 mm × 25.0 mm. The columns from left to right correspond to real, imaginary, and modulus of the waves. Note that the scale bar of the modulus images is different from that of the real and imaginary images. The parameters for the X wave are $a_0 = 0.05mm$ and $\zeta = 4.75^o$, and for the subsonic wave are $\xi = 100.53m^{-1}$ and $\zeta = 4.75^o$.

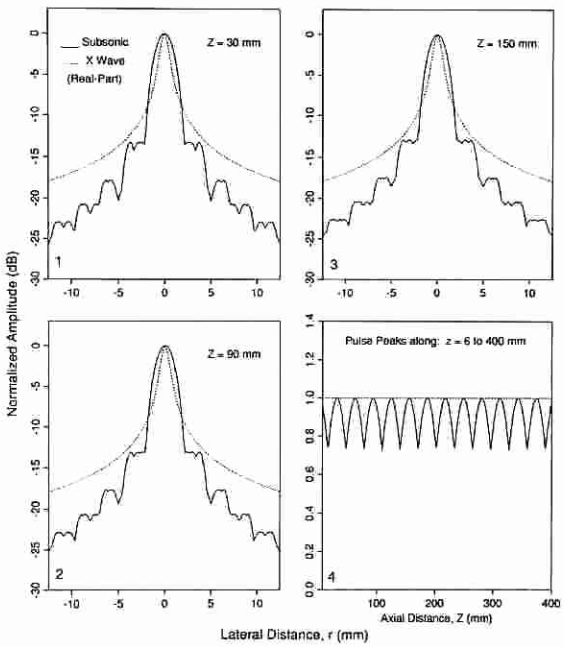


**Figure 2.** Line plots of the maximum envelope of A-lines of the real part of the X wave (dotted lines) and the subsonic wave (solid lines) shown in Fig. 1 at 3 axial distances: $z$ = (1) 30, (2) 90, and (3) 150 mm, versus the radial distance. Peak of the waves versus the propagation distance from 6 to 400 mm is shown in Panel (4). It is seen that the subsonic wave has lower sidelobes and the peak of the wave oscillates as it propagates. The waves are assumed to be produced with an infinite aperture and energy.

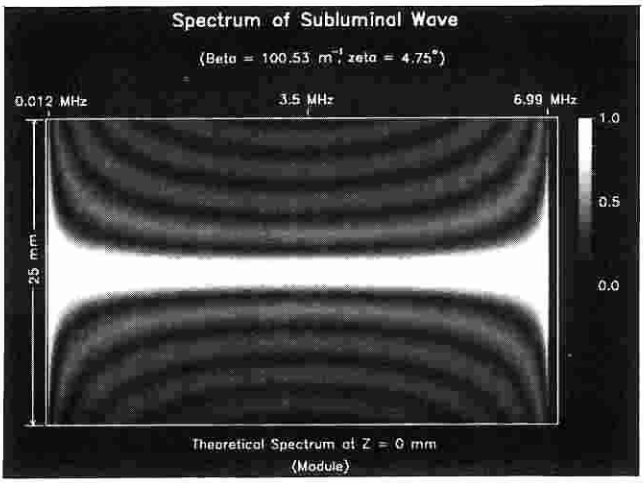


**Figure 3.** The modulus of the spectrum of the subsonic wave in Fig. 1 (see Eq. (3)) at the axial distance, $Uz = 0$. The horizontal direction represents frequency and the vertical direction represents the radial distance. With the parameters of the subsonic wave shown in Fig. 1, the frequency components are limited between 0.012 MHz and 6.99 MHz with a central frequency of 3.5 MHz.

$z - c_1 t$ and $z - c_2 t$, where $c_1$ and $c_2$ are different constants. For the subsonic wave (Eq. (2)), $c_1 = c \cos \zeta < c$ (subsonic) in the amplitude term and $c_2 = c/\cos \zeta > c$ (supersonic) in the phase term.

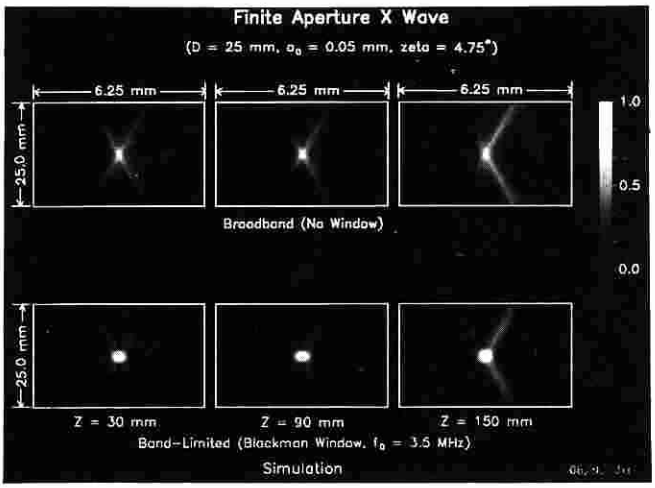


**Figure 4.** X waves produced at 3 axial distances ($z$ = 30 (left column), 90 (middle column), and 150 mm (right column)) with a transducer of diameter of 25 mm. The images in the top row are produced with a transducer of infinite bandwidth, while the images in the bottom row are produced with a transducer of the Blackman window type of transfer function with a central frequency of 3.5 MHz and a $-6$-dB relative bandwidth of about 81%. The dimension of the images and the parameters of the waves are the same as those in Fig. 1.

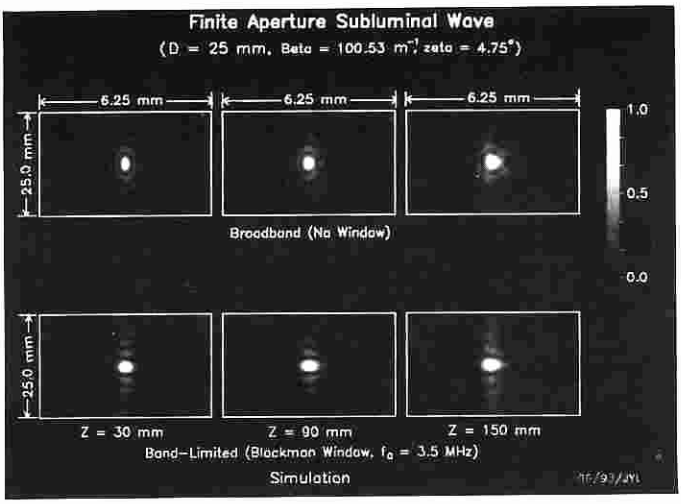


Figure 5. The subsonic (or subluminal) waves produced at 3 axial distances ($z$ = 30 (left column), 90 (middle column), and 150 mm (right column)) with a transducer of diameter of 25 mm. This figure has the same format as that of Fig. 4 and the parameters of the waves are the same as those in Fig. 1.

## RESULTS

A plot of Eqs. (1) and (2) at $z = 0$ is shown in Fig. 1. The parameters of the X wave and the subsonic wave are adjusted so that they have comparable mainlobe sizes. For the X wave, $a_0$ = 0.05 mm and $\zeta = 4.75^{\circ}$. And for the subsonic wave, $\zeta = 4.75^{\circ}$ and $\xi =$

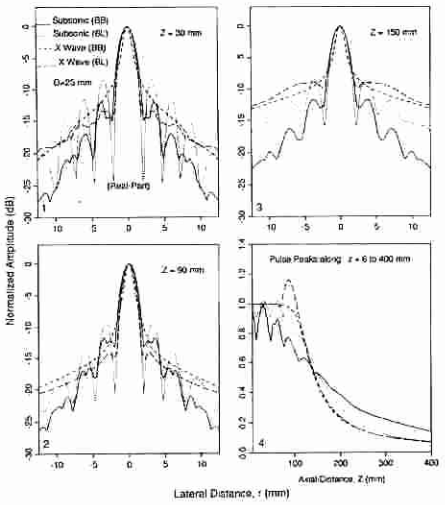


Figure 6. Line plots of the maximum envelope of A-lines of the real part of the X waves and the subsonic waves produced with a finite aperture transducer (25 mm in diameter) in Figs. 4 and 5, respectively, versus the radial distance. The plots are obtained at 3 axial distances: $z$ = (1) 30, (2) 90, and (3) 150 mm. Peak of the waves versus the propagation distance from 6 to 400 mm is shown in Panel (4). "BB" and "BL" represent broadband and band-limited waves, respectively. Solid and dotted lines represent the broadband and the band-limited subsonic waves, respectively. Dashed and long dashed lines represent the broadband and the band-limited X wave, respectively.

100.53 $m^{-1}$. A line plot that corresponds to the real part of the waves in Fig. 1 is shown in Fig. 2. The difference of the sidelobes between the two waves is clearly seen. The sidelobes are obtained by plotting the maximum of each A-line (lines that are parallel to the wave axis (in horizontal direction of Fig. 1)) versus the radial distance of the beams. The oscillations of the peaks of the subsonic wave as it propagates are also obvious. The shape of the modulus of the subsonic wave in Fig. 1 is composed of concentric ellipses. That is why the peak of the subsonic wave propagates slower than the speed of sound.

The modulus of the spectrum of the subsonic wave is shown in Fig. 3. It has clear lower and upper cut off frequencies (see Eq. (3)). This is different from other localized waves[10] whose frequency components extend to infinity. The lower and upper cut off frequencies of the subsonic wave are given by $f_l = (1 - \cos\zeta)f_0$ and $f_h = (1 + \cos\zeta)f_0$, respectively, where $f_0 = \xi c/(2\pi \sin^2\zeta)$ is the central frequency. The spectrum in Fig. 3 is obtained at $z = 0$ for various radial distances, $r$ (in the vertical direction of the figure). The lower and upper cut off frequencies can be calculated with the parameters of the subsonic waves in Fig. 1: $f_l = 0.012$ MHz and $f_h = 6.99$ MHz (the central frequency is $f_0 = 3.5$ MHz). The relative bandwidth ($(f_h - f_l)/f_0 = 2\cos\zeta$) of the spectrum is extremely large (about 199%).

In practical applications, waves must be produced with transducers of finite apertures and finite relative bandwidth. X waves (Fig. 4) produced by the transducer that has either a finite aperture (diameter $D = 25$ mm) or a finite aperture plus finite lower and upper cut off frequencies have been simulated using the Rayleigh-Sommerfeld diffraction formula.[18] The envelope of the real part of the X waves is displayed in Fig. 4. For the broadband X wave, a flat frequency response of the transducer is assumed. The lower and upper cut off frequencies for the band-limited X waves are 0 and 7.0 MHz, respectively, which correspond to the frequencies at zeroes of the Blackman window function.[17] The Blackman window has a central frequency of 3.5 MHz and its $-6$-dB relative bandwidth is about 81% of the central frequency. The simulated finite aperture subsonic wave is shown in Fig. 5 in the same format as Fig. 4. The parameters for the X wave and the subsonic wave are the same as those in Fig. 1.

Line plots of Figs. 4 and 5 are shown in Fig. 6 in the same format as Fig. 2. It is seen that sidelobes of the subsonic wave increase as the bandwidth decreases. For the X wave, sidelobes reduce with the bandwidth slightly.

Changes in the characteristics of the sidelobes of the subsonic wave with several Blackman window functions are shown in Fig. 7. These Blackman windows are shown in Fig. 8. It is noted that as the base bandwidth of the Blackman window function decreases from 14 MHz to 7 MHz, the sidelobes are increased dramatically (the base bandwidth is determined by the frequencies that correspond to the zeroes of a Blackman window function).

## CONCLUSION

Sidelobes of limited diffraction beams are higher than those of conventional focused beams at their focuses. One way to reduce the sidelobes is to use localized waves that are non-spreading and propagate with only local deformations. However, to take advantage of the low sidelobes of localized waves, the transducers used to produce these waves must have a large relative bandwidth (at least 162% $-6$-dB relative bandwidth in the above example, see Fig. 7). Perhaps PVDF transducers, that have large bandwidth, could be used to produced low sidelobe localized waves.

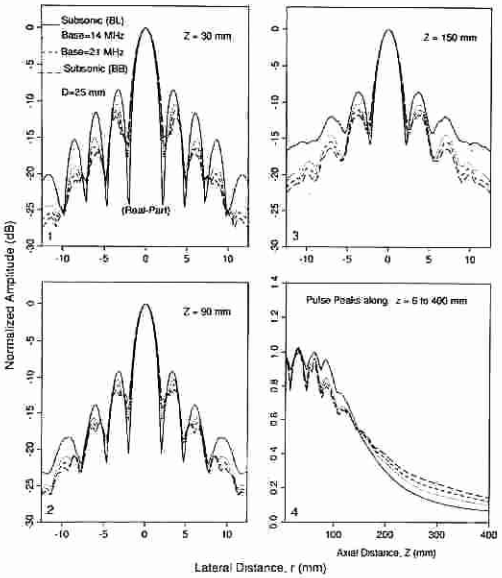


**Figure 7.** Line plots of the maximum envelope of A-lines of the real part of the subsonic waves produced with a finite aperture transducer (25 mm in diameter) versus the radial distance showing the change of sidelobes with transducer bandwidth. The figure has the same format as that of Fig. 6. "Subsonic (BL)" (solid lines) and "Subsonic (BB)" (long dashed lines) represent the subsonic waves obtained with the transducer that has a transfer function of the Blackman window type centered at 3.5 MHz, and are repeated from Fig. 6 for comparison. These plots correspond to the base bandwidths (the bandwidth between the two zeroes of the Blackman window, see Fig. 8) of 7.0 MHz and infinity respectively. Dotted and dashed lines represent the subsonic waves produced by the transducer of 14 MHz and 21 MHz base bandwidths, respectively (see Fig. 8).

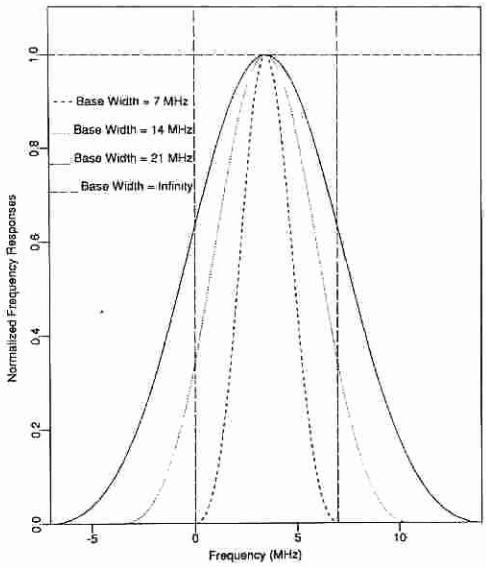


**Figure 8.** Examples of Blackman windows of different bandwidths: 7.0 MHz (dashed line), 14.0 MHz (dotted line), 21.0 MHz (solid line), and infinity (long dashed line). The two vertical dashed lines represent the lower and higher cut off frequencies of the subsonic waves calculated by using the parameters in Fig. 1. The −6-dB bandwidth of the Blackman window is about 41% of the base bandwidths above.

## ACKNOWLEDGMENTS

The authors appreciate the secretarial assistance of Elaine C. Quarve. This work was supported in part by grants CA 43920 and CA 54212 from the National Institutes of Health.

## REFERENCES

1. J. Durnin, Exact solutions for nondiffracting beams. I. The scalar theory, *J. Opt. Soc. Am.* 4(4):651–654 (1987).
2. Jian-yu Lu and J.F. Greenleaf, Nondiffracting X waves — exact solutions to free-space scalar wave equation and their finite aperture realizations, *IEEE Trans. Ultrason., Ferroelec, Freq. Cont.* 39(1):19–31 (Jan., 1992).
3. Jian-yu Lu and J.F. Greenleaf, Experimental verification of nondiffracting X waves, *IEEE Trans. Ultrason., Ferroelec., Freq. Contr.* 39(3):441–446 (May, 1992).
4. Jian-yu Lu and J.F. Greenleaf, Ultrasonic nondiffracting transducer for medical imaging, *IEEE Trans. Ultrason., Ferroelec., Freq. Contr.* 37(5):438–447 (Sept., 1990).
5. Jian-yu Lu and J.F. Greenleaf, Pulse-echo imaging using a nondiffracting beam transducer, *Ultrasound Med. Biol.* 17(3):265–281 (May, 1991).
6. Jian-yu Lu, and J.F. Greenleaf, Evaluation of a nondiffracting transducer for tissue characterization, [IEEE 1990 Ultrasonics Symposium, Honolulu, HI, Dec. 4–7, 1990], *IEEE 1990 Ultrason. Symp. Proc.* 90CH2938-9, 2:795–798 (1990).
7. Jian-yu Lu and J.F. Greenleaf, Producing deep depth of field and depth-independent resolution in NDE with limited diffraction beams, *Ultrason. Imag.* 15(2):134–149 (April, 1993).
8. R.W. Ziolkowski, Localized transmission of electromagnetic energy, *Phys. Rev. A.* 39(4):2005–2033 (Feb. 15, 1989).
9. J. Ojeda-Castaneda and A. Noyola-Iglesias, Nondiffracting wavefields in grin and free-space, *Microwave and Optical Tech. Lett.* 3(12):430–433 (Dec. 12, 1990).
10. Jian-yu Lu and J.F. Greenleaf, Biomedical ultrasound beamforming, *Ultrasound Med. Biol.* (to be published in 1994).
11. J.N. Brittingham, Focus wave modes in homogeneous Maxwell's equations: transverse electric mode, *J. Appl. Phys.* 54(3):1179–1189 (1983).
12. R.W. Ziolkowski, Exact solutions of the wave equation with complex source locations, *J. Math. Phys.* 26(4):861-863 (April, 1985).
13. R.W. Ziolkowski, D.K. Lewis, and B.D. Cook, Evidence of localized wave transmission, *Phys. Rev. Lett.* 62(2):147–150 (Jan. 9, 1989).
14. R. Donnelly and R.W. Ziolkowski, A method for constructing solutions of homogeneous partial differential equations: localized waves, *Proc. R. Soc. Lond. A.* 437:673–692 (1992).
15. R. Donnelly and R.W. Ziolkowski, Designing localized waves, *Proc. R. Soc. Lond. A.* 440:541–565 (1993).
16. R. Donnelly, D. Power, G. Templeman and A. Whalen, Graphic simulation of superluminal acoustic localized wave pulses, *IEEE Trans. Ultrason., Ferroelec., Freq. Contr.* 41(1):7–12 (Jan., 1994).
17. A.V. Oppenheim and R.W. Schafer, *Digital signal processing.* Prentice-Hall, Inc., Englewood Cliffs, NJ, ch. 5 (1975).
18. J.W. Goodman, *Introduction to Fourier Optics.* McGraw-Hill, New York, chs. 2–4 (1968).